Advanced Composite Materials
Publication details, including instructions for authors and subscription information:
http://www.tandfonline.com/loi/tacm20

Experimental study of composite T-joints under tensile and shear loading

P. B. Stickler & M. Ramulu

Version of record first published: 02 Apr 2012.

To cite this article: P. B. Stickler & M. Ramulu (2006): Experimental study of composite T-joints under tensile and shear loading, Advanced Composite Materials, 15:2, 193-210

To link to this article: http://dx.doi.org/10.1163/156855106777873914

Adv. Composite Mater., Vol. 15, No. 2, pp. 193–210 (2006)

Also available online - www.vsppub.com

Experimental study of composite T-joints under tensile and shear loading *

P. B. STICKLER [1,†] and M. RAMULU [2]

[1] *The Boeing Company, P. O. Box 3707, MC: 0R-CC, Seattle, WA 98124-2207, USA*
[2] *University of Washington, Department of Mechanical Engineering, Seattle, WA 98195, USA*

Received 14 October 2004; accepted 6 October 2005

Abstract—An experimental study of a new type of composite T-joint with transverse stitching was conducted under tensile and shear loading. Fixtures were designed to load the T-joint specimens under simple support and fixed support boundary conditions, respectively. During experimentation, load–displacement and strain–load measurements were recorded and post-failure analysis was accomplished on failed specimens using optical microscopy. T-joint behavior under simple-support tension boundary conditions was shown to be linear up to initial failure. Specimens failed initially due to matrix cracking at the fillet region of the web-to-flange interface. Onset of ultimate failure was attributed to fiber insertion bridging leading to insertion breakage and pullout. The mechanical behavior under an applied shear load was marked by nearly linear behavior up to ultimate failure. Specimens fail by interfacial matrix cracking at the web-to-flange interface leading to T-joint catastrophic failure with complete separation of the web and flange.

Keywords: Composite T-joint; testing; failure analysis; transverse stitching.

1. INTRODUCTION

Efficient joining methods are required to reduce the structural weight and manufacturing cost of composite load-bearing structures. Joints tend to be the weakest part of the structure and thus may attribute to significant weight penalties [1]. There are many types of composite joints used in industry. In-plane joints include single lap, double lap, and butt joints. Out-of-plane joints are typically T-joints, and consist of orthogonal web and flange members. In T-joint applications, the web provides an attachment point for an adjacent member such as a bulkhead or frame. In the case of a marine structure, the flange would be attached to the hull and in the case of an aerospace application, the flange would be attached to the fuselage or

*Edited by the JSCM.

†To whom correspondence should be addressed. E-mail: patrick.b.stickler@boeing.com

wing skin. In-service loads on this type of joint include flexure, tension, and out-of-plane or rail shear. Structural T-joints may be bonded or bolted. Bolted joints are damage tolerant but create high stress concentrations at the hole locations and composites have notably poor bearing strength [2]. Methods of bonding composites include co-curing, co-bonding, and secondary bonding. Bonded joints tend to be more structurally efficient but have low interlaminar shear and peel strengths [3].

One method of improving the interlaminar shear and peel strength of composite joints is through the use of transverse stitching. This technique has been shown to improve the ultimate strength of single lap joints in tension by 20% [4]. Primary structural application of composite materials requires detailed consideration of initial failure and ultimate load-carrying capability and associated damage tolerance. Shenoi and Violette [5] studied the effect of T-joint geometry under out-of-plane loading for hull bulkhead structures. A preliminary design tool was proposed based on experimental and numerical analysis. Composite T-joint sandwich structures were evaluated under pull-off loads by Theotokoglou [6]. In these experiments the load–displacement behavior was shown to be nonlinear. Both geometric nonlinearities and nonlinear material behavior were present. The geometric nonlinearities were caused by out-of-plane loading of the flange; the material nonlinearities were attributed to plastic yielding of the interfacial adhesive. Failures were shown to occur at the web-to-flange interface. Phillips and Shenoi [7] investigated the damage tolerance of laminated composite T-joints. Mechanical behavior was investigated under off-axis pull-off and three-point bend load conditions. T-joint failure progressed in a series of steps with increased load. Failures were shown to occur by delamination in the angle plys and fillet resin region at the web-to-flange interface.

Transverse stitching has been used as a means of suppressing delaminations in bonded T-joints and T-stiffeners. Young and Chuang [8] investigated T-joints fabricated using resin transfer molding and transverse stitching of the flange at an offset distance form the web-to-flange interface. T-joint ultimate failure under tension loading was shown to be improved using transverse stitching. Z-fibers or Z-pins have been investigated as a means of improving the performance of T-stiffeners by Freitas *et al.* [9]. Stiffener pull-off experiments were conducted and Z-fibers were shown to effectively delay the onset of initial failure and improve damage tolerance. A new low cost T-joint with transverse stitching, using a fiber insertion process and dry fabric preforms, has been investigated by Stickler, Ramulu, *et al.* [10, 11] under flexure loading. In the case of one-sided stitching (referred to as fiber insertion), continuous fiber tows are inserted directly at the web-to-flange interface, providing a mechanism for load transfer and an automated method of joining dry fiber preforms. In these investigations, experiments were conducted and failure mechanisms were identified. Initial failure was shown to occur by interfacial matrix cracking. Ultimate failure occurred by fiber insertion breakage and pullout.

The motivation of the present research was to characterize the performance of the fiber insertion process under tension and shear loading and to elucidate any potential

limitations of this new low-cost construction method prior to application. In this paper, an experimental study of a new type of composite T-joint with transverse stitching was conducted under tensile and shear loading for the first time. The mechanical behavior and failure mechanisms were investigated using the recorded load–displacement and strain–load data. A post-failure analysis was performed to identify failure mechanisms; damage progression was characterized under increased load.

2. EXPERIMENTAL SETUP AND PROCEDURE

2.1. Specimen fabrication

The T-joint specimens used in this evaluation were fabricated from T-300-3k-4h satin weave, two-dimensional dry fabric preforms manufactured by Albany International Techniweave, Inc. Hexcel IM7 6k tow fiber insertions were used for transverse stitching. Specimen preforms were stitched using the fiber insertion process prior to resin transfer molding (RTM) consolidation with PR520 toughened epoxy resin. The fiber insertion process is accomplished using a fiber tow and a special needle. The needle is inserted into the preform to a predetermined depth and extracted leaving the tow loop in place. An insertion pitch of four stitches/cm was used and two rows of fiber insertions were placed symmetrically 0.125 cm from the web centerline. The fiber insertions pass through the flange preform and penetrate the web to a nominal depth of 12.5 mm. The web is fabricated using a quasi-isotropic 24 ply $[0/45]_{6s}$ dry fabric preform and the flange is fabricated from a near quasi-isotropic 22 ply $[(0/45)_5/0]_s$ dry fabric preform. Individual plies are held together with a small amount of tackifier to facilitate handling prior to resin transfer molding.

During RTM processing, the PR520 specimens are cured by preheating the resin to 80°C and then sending it through a heat exchanger to reach an injection temperature of 163°C. The RTM mold is preheated to 163°C. Next, the resin is transferred at 517 kPa while the mold is under vacuum. After fiber wet-out is ensured, the specimens are cured for 120 min at 180°C, and demolded. The typical cured specimen fiber volume fraction is 55%. Figure 1a shows a typical tension specimen with strain gage instrumentation. Figure 1b shows a typical rail shear specimen with strain gage instrumentation and fixture attachment holes.

2.2. Tension fixture

Tension experiments were performed on the T-joint specimens using the experimental setup shown in Fig. 2a. A steel fixture was designed to load the specimens in tension under simple support boundary conditions. Prior to loading, specimens were placed in the fixture and the web was clamped using static load frame hydraulic grips. Specimen webs were gripped 3.8 cm from the web-to-flange interface. The

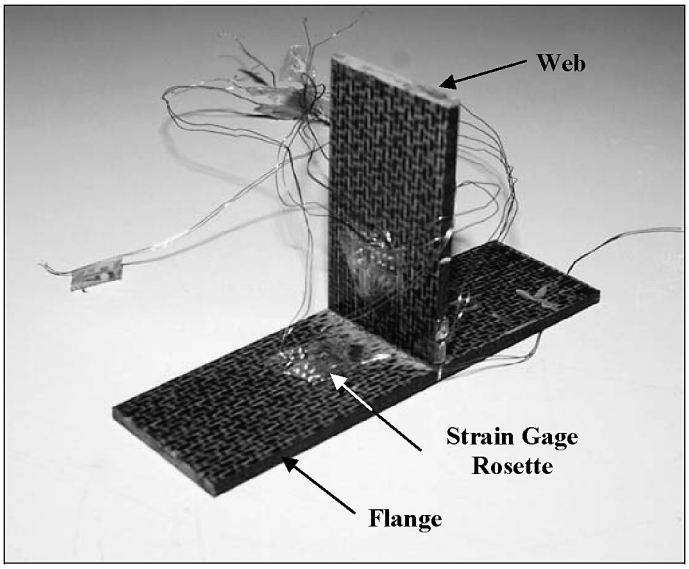

(a)

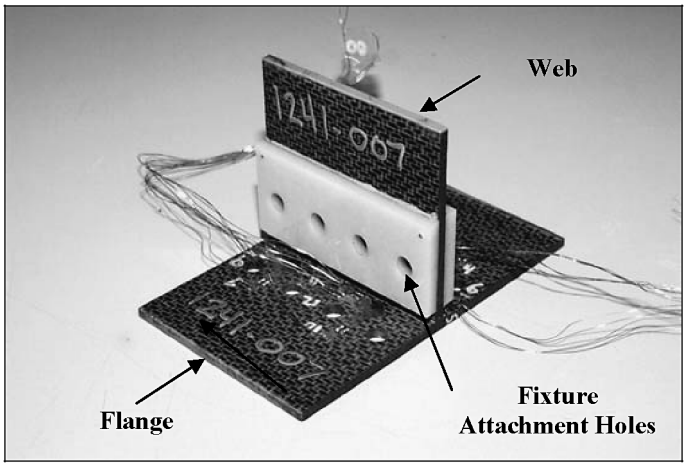

(b)

Figure 1. Typical T-joint specimens: (a) tension specimen showing instrumentation and (b) shear specimen showing instrumentation and fixture attachment holes.

simple supports for the flange were located 4.5 cm from the web centerline, placing the web in tension and the flange in flexure.

2.3. Shear fixture

T-joint specimens are trimmed to final dimensions and the specimen webs are tabbed using Grade G-10 glass/epoxy. Tabs are used on the web to prevent local failure at the fixture attachment locations. Figure 2b shows the steel rail shear experimental

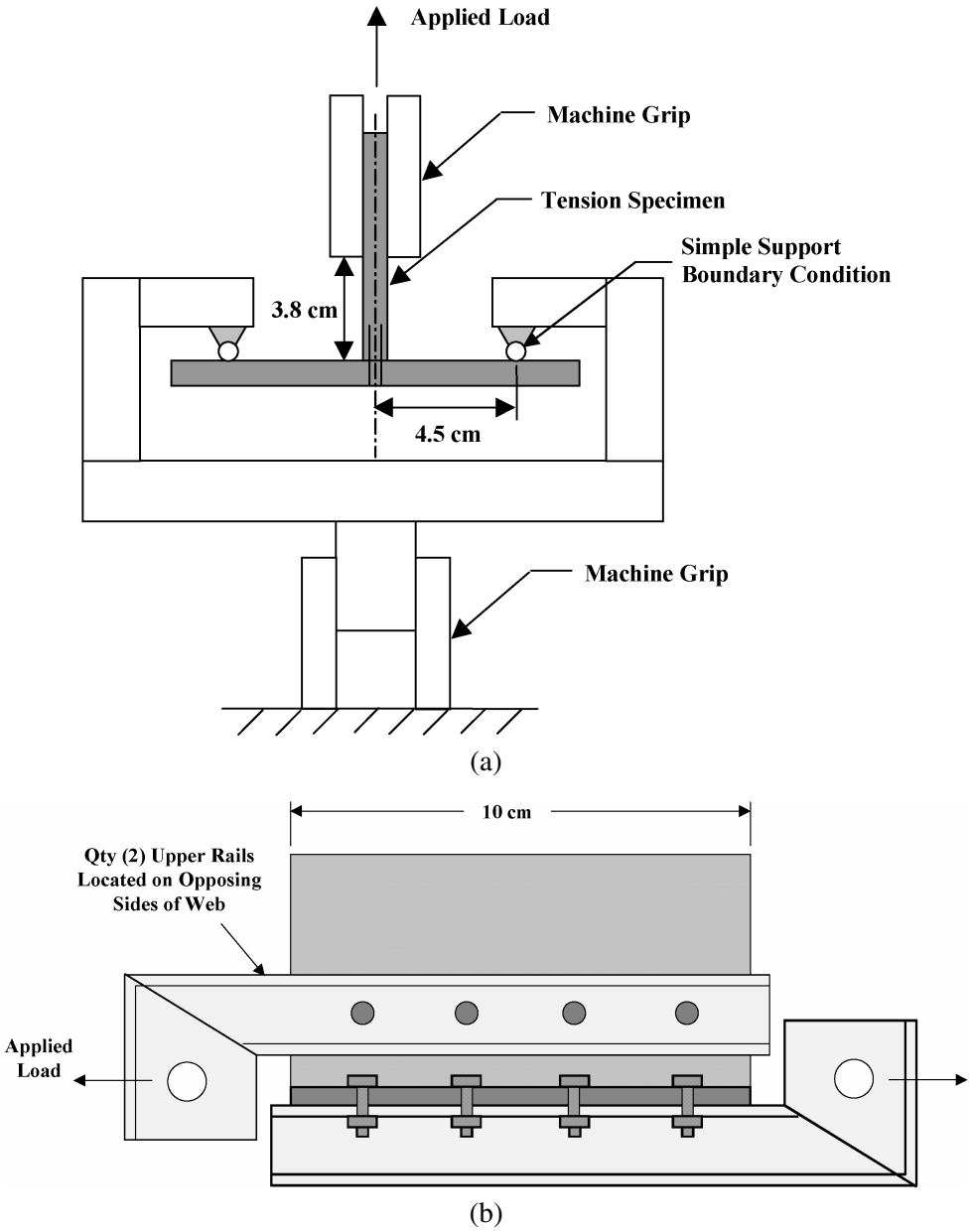

Figure 2. Experimental setup: (a) tension front view and (b) rail shear side view.

test fixture. The fixture is designed with a single line of action to ensure pure shear loading of the specimen web-to-flange interface. Upper rails are attached to opposing sides of the web, ensuring symmetric loading of the interface region. The flange of each T-joint specimen is bolted to the fixture backing plate at four

locations along the width on each side of the web and at four locations on the web using 9.5 mm Grade 8 steel bolts.

2.4. Experimental procedure

The specimens were tested in an Instron Model 1332 static load frame using displacement control. Specimens were loaded at a rate of 1.25 mm/min. A hydraulic grip pressure of 25 kN was used and each specimen was preloaded to 50 N in the case of tensile test and 400 N in shear. Tension experiments were terminated after a 50 percent drop in load was detected. A total of five tension and five shear experiments were conducted under room temperature ambient conditions. Both load–displacement and strain–load data were recorded for all specimen configurations. Load–displacement data was measured using an Instron 2518-610 load cell. During testing, load was applied parallel to the longitudinal axis of the specimen in both experiments. Processing of load–displacement data was accomplished using an MTS model 458.20 controller and a National Instruments model SCXI-1000 conditioner. Data were recorded using a PC and LabVIEW version 5.1 data acquisition and control software.

Strain measurements were taken using Micro-Measurements strain gages [12]. Two WA-06-120WR-350 three element 45 degree rectangular stacked rosettes and two EA-06-062AQ-350 uniaxial gages were selected for these experiments. For the tension specimens, gages were bonded to the upper surface of the flange and to the upper surface and edge of the web using M-bond 200 cement as shown in Fig. 3a. Three-element stacked rosettes were positioned 1.25 cm from the web centerline on the flange and 1.25 cm from the flange on the web. The uniaxial gages were located on the web edge at distances of 0.625 cm and 1.25 cm from the flange. For the shear specimens, strain gages were positioned ± 1.25 cm from the web centerline equidistant from the fastener holes to avoid near field strains associated with fastener hole stress concentrations as shown in Fig. 3b. Strain gages were not placed on the web due to the requirements for tabs at this location. All gages have a resistance of 350 ohms and a gage factor of 2.1.

2.5. Post failure analysis

Failed T-joints are sectioned to establish the failure mechanisms and the evolution of damage leading to ultimate failure. Optical micrographs are taken using an Olympus BH-2 Metallurgical Microscope with a magnification of $20\times$. Digital images are acquired using a Nicon COOLPIX 950 Camera. Prior to examination, specimens are potted using Buehler SAMPL-KWICK Compound. An Automet 2 Polisher and a staged polishing process are used to prepare specimens for optical micrograph. A series of diamond suspension fluids are used with 15, 9, 3, and 0.5 grit.

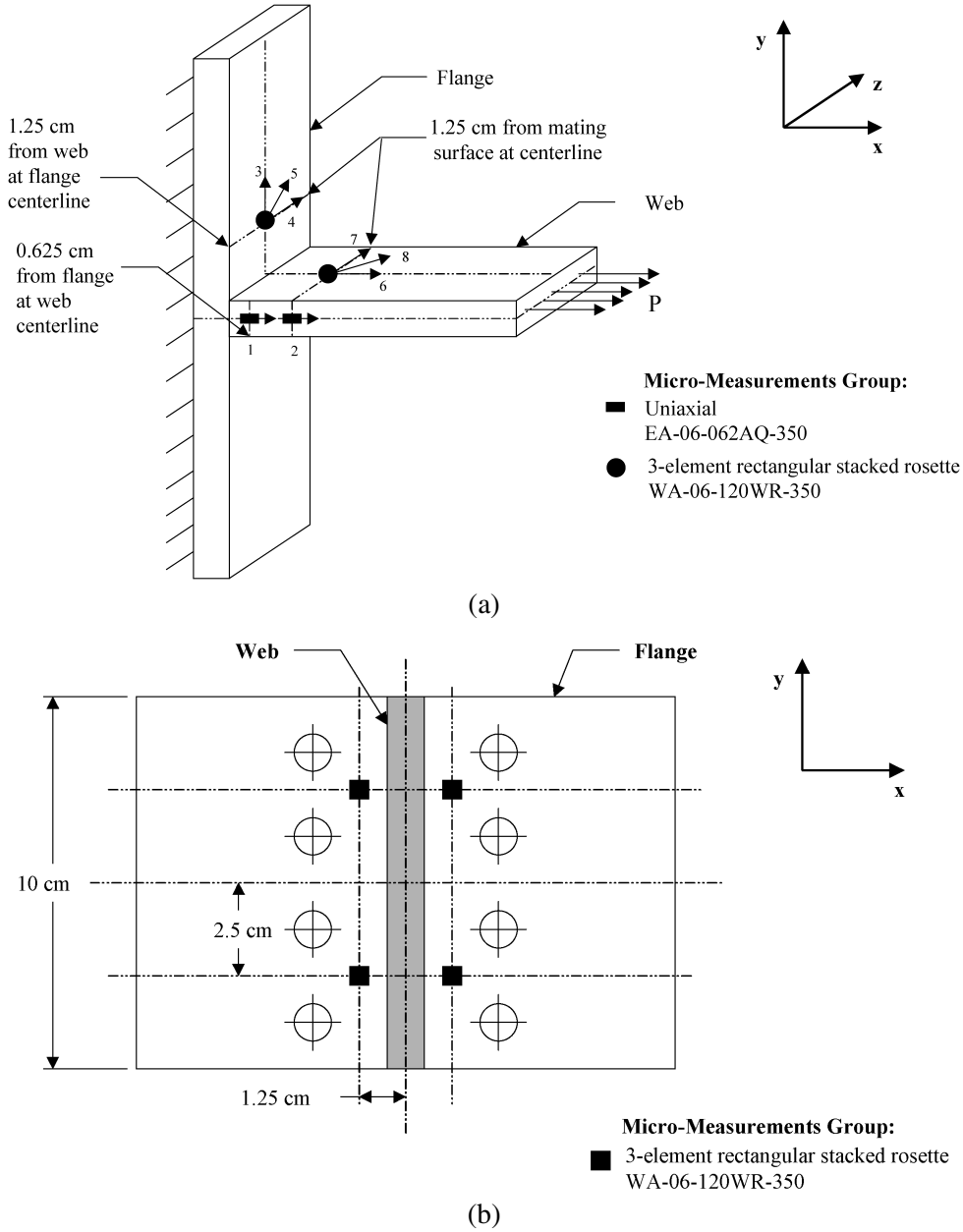

Figure 3. Specimen instrumentation schematic: (a) tension and (b) rail shear.

3. RESULTS

A summary of damage initiation load and ultimate damage load for each tension experiment is shown in Table 1. Shown are the initial and ultimate damage loads including mean, standard deviation (SD), and coefficient of variation (CoV). The

Table 1.
Initial and ultimate damage load summary under tension

Tension specimen	Web thickness (mm)	Flange thickness (mm)	Specimen width (mm)	Damage initiation load (kN)	Ultimate load (kN)
T 1	4.78	4.80	50.85	5.37	5.74
T 2	4.80	4.80	50.80	5.38	6.05
T 3	4.83	4.78	50.83	5.38	5.83
T 4	4.83	5.26	50.75	5.81	5.92
T 5	4.78	4.85	50.62	3.55	5.16
Mean	4.80	4.90	50.77	5.10	5.74
Std Dev.	0.03	0.20	0.09	0.89	0.34
CoV (%)	0.5	4.2	0.2	17.4	6.0

Table 2.
Initial and ultimate damage load summary under shear

Rail shear specimen	Web thickness (mm)	Flange thickness (mm)	Specimen width (mm)	Damage initiation load (kN)	Ultimate load (kN)
S 1	5.23	4.72	101.40	30.93	38.30
S 2	5.21	4.88	101.47	36.30	36.30
S 3	5.16	4.85	101.83	36.25	36.25
S 4	5.26	4.83	101.78	28.43	33.63
S 5	5.18	4.87	101.37	29.58	29.58
Mean	5.21	4.83	101.57	32.30	34.81
Std. Dev.	0.04	0.06	0.22	3.74	3.36
CoV (%)	0.8	1.3	0.2	11.6	9.7

average initial damage load is 5.10 kN; the average ultimate damage load is 5.74 kN. A moderate amount of scatter was noted in the initial and ultimate damage load. The CoV at initial and ultimate failure are 17.4 percent and 6.0 percent, respectively. It was noted that specimen T5 failed prematurely. All specimens exhibited additional load-carrying capability beyond initial failure.

The damage initiation load and ultimate damage load for the rail shear experiments are provided in Table 2. The average initial damage load was determined to be 32.30 kN and the average ultimate damage load is 34.81 kN. The CoV at initial failure load is 11.6% and 9.7% at ultimate failure. A moderate amount of scatter was noted in the load data. It was noted that specimens S2, S3, and S5 failed catastrophically at the damage initiation load. Specimens S1 and S4 exhibited additional load carrying capability beyond initial failure. Complete separation of the web and flange were observed in Specimens S1, S2, and S4.

A combined load–displacement plot under tensile loading is shown in Fig. 4a. The T-joints behave nearly linearly up to initial failure. During loading, audible

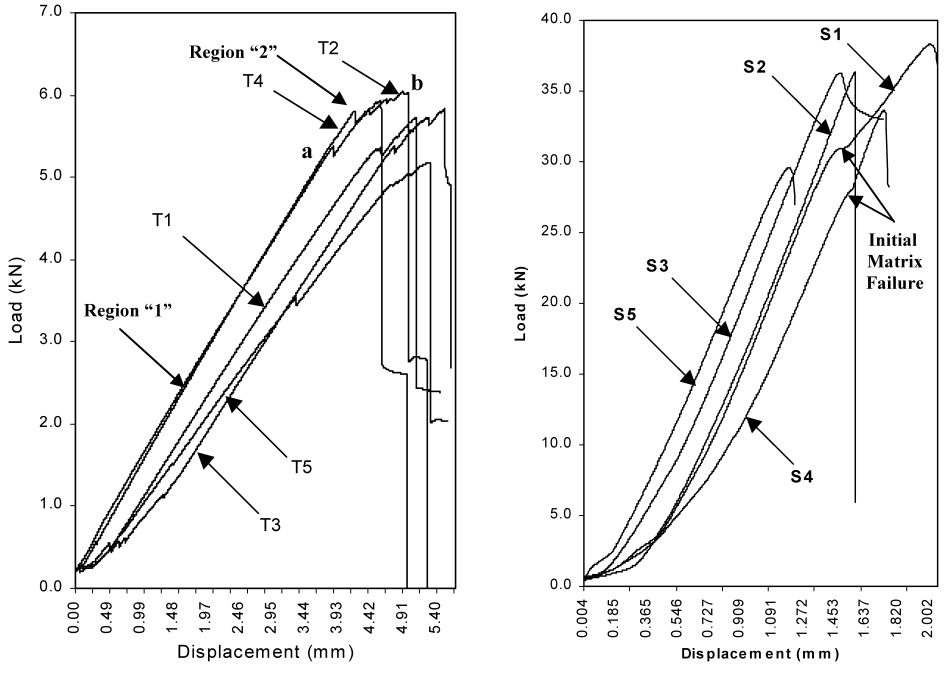

Figure 4. Load–displacement plots: (a) tension and (b) shear.

cracking was noted at the onset of initial failure for each specimen. At initial failure, a distinct drop in load–displacement was noted. A second region of linearity was observed with increased load after initial failure. A large drop in load–displacement represents catastrophic T-joint failure. In each case, the load dropped by greater than 50 percent at ultimate failure. The initial nonlinearity noted in the load–displacement plot is indicative of specimen fixture seating. An initial preload of 50 N was applied to the specimens as noted above. The load–displacement for specimens T2 and T4 matched very well. Specimens T1 and T3 had a slope within 5 percent of that of specimens T2 and T4, but experienced additional seating. Again, specimen T5 had a low initial failure. Figure 4b shows a combined load–displacement plot for the T-joints under rail shear loading. The T-joints behave nearly linearly up to initial failure with nonlinearity occurring at the onset of matrix failure as indicated by a leveling off of the load–displacement curve just prior to ultimate failure. During loading, audible matrix cracking was noted at the onset of initial failure for each specimen. A complete separation of the web and flange is indicated by the large drop in load–displacement at the end of each experiment. An initial matrix crack may be observed in specimens S1 and S4 as shown by a drop in the load–displacement prior to ultimate failure. All specimens had a consistent slope but experienced varying amounts of nonlinearity upon initial loading. The initial nonlinearity noted in the load–displacement plot is indicative of specimen fixture seating. An initial preload of 400 N was applied

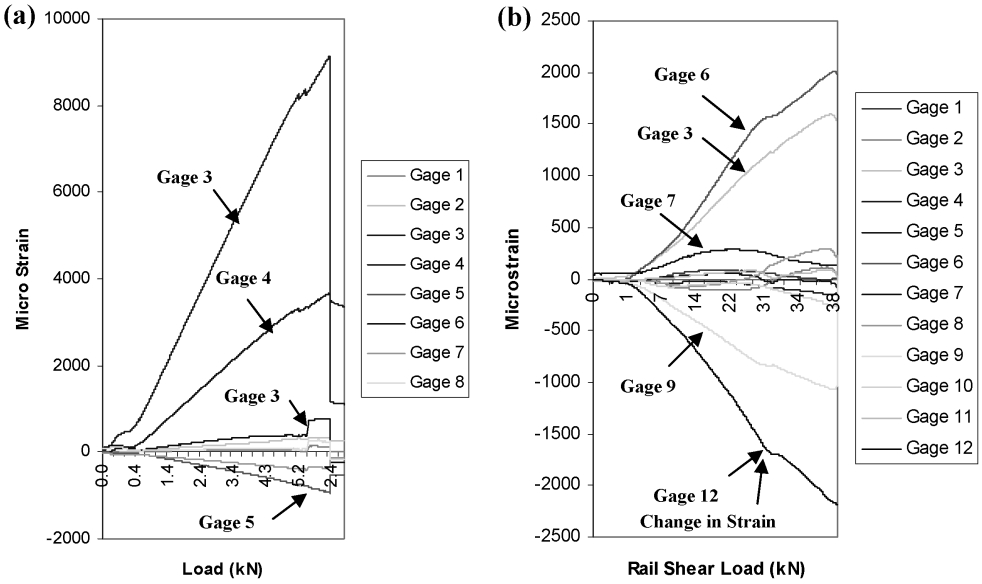

Figure 5. Typical specimen strain–load plot: (a) tension and (b) shear.

to the specimens as noted above. The specimen seating may be attributed to small misalignments in fastener hole location and/or deviations in fabricated specimen geometric tolerances. The presence of fixture seating indicates that an increased preload to 5 kN may be warranted in future experiments. A post-failure examination of the fixture attachment holes was conducted to ensure local bearing failure did not occur in the T-joint during loading. This examination did not reveal any fastener hole bearing damage.

Figure 5a shows the strain–load plots for a typical tension specimen. A peak average tensile strain of 9620 $\mu\varepsilon$ was recorded at strain gage location three at ultimate failure. This peak strain does not exceed the laminate tensile failure strain of 13930 $\mu\varepsilon$ reported previously by Stickler *et al.* [13], indicating no web failure occurred during static flexural loading. A peak average compressive strain of -980 $\mu\varepsilon$ was recorded in strain gage location five. The experimentally determined laminate compressive failure strain of 12450 $\mu\varepsilon$ was not exceeded during static tensile loading, indicating that the web laminate did not fail in compression. A discrete jump in strain is noted in direct correspondence to initial matrix cracking, as indicated at point 'a' on the load–displacement plot. This may be attributed to load redistribution within the web and flange after initial matrix interface cracking. Figure 5b shows the far field strain–load plots for a typical shear specimen. Peak tensile and compressive strains were recorded in the 45-degree gage locations for each 3-element rosette. Average peak tensile strains of 1810 $\mu\varepsilon$ are recorded at strain gage location 6. An average peak surface compressive strain of -1930 $\mu\varepsilon$ was recorded at gage location 12. A discrete change in strain is noted in direct correspondence to initial matrix cracking as indicated on the load–displacement

plots. This may be attributed to load redistribution to the fiber insertions within the web and flange after initial matrix interface cracking. The peak laminate surface shear strain, γ_{xy} is determined using the rosette strain gage equations. Using recorded strains gage location 10, 11, and 12, the laminate shear strain is determined to be 4240 $\mu\varepsilon$. Average peak measured far field laminate axial and shear strains are well below that of the allowable laminate strains as presented previously by Stickler *et al*. [13] indicating no failure of the T-joint laminates. Instead, failure occurred locally at the web-to-flange interface.

The optical micrographs for failed tension specimen T3 is shown in Fig. 6a. Nonuniformity of the fiber prefoms at the web-to-flange interface is visible. This nonuniformity creates a resin-rich region. Also shown are the radius fillets created by the RTM tool during processing. Matrix cracks are clearly present at the fillets in this region and extend along the web-to-flange interface. Cracks are also shown extending along the fiber insertion. A flange sublaminate crack is visible between the fiber insertions. Optical micrographs of failed shear specimen S3 is shown in Fig. 6b. In the optical micrograph of specimen S3, the IM7 fiber insertions are clearly visible. Also shown is an interfacial matrix crack at the 'resin-rich' web-to-flange interface. The crack extends across the entire interface.

4. DISCUSSION

The mechanical behavior under tensile loading with simple support boundary conditions may be divided into two distinct regions, as shown in Fig. 4a. In region one, the flange deflects elastically under increased load up to point 'a' on the load displacement plot. Region two is marked by additional linear behavior up to point 'b' or ultimate failure. The fiber insertions are loaded symmetrically in tension. Near the initial damage load, the fillet region at the web-to-flange interface exceeds that of the neat resin tensile strength. At the damage initiation load, a crack initiates in the fillet region and propagates to the fiber insertions. This causes a marked drop in the load–displacement record as shown at point 'a' of Fig. 4a. A 3–5 percent drop in load was noted at initial T-joint failure. A similar response is recorded in the strain–load plot, as shown in Fig. 5a. The direction and extent of damage may be represented schematically based on the optical micrographs of the failed tension specimens. Figure 7a shows the initial crack forming at the resin-rich fillet region; Fig. 7b shows the crack propagating along the interface to the fiber insertions. Increased load beyond initial damage, defined as region 2 of the load–displacement plot of Fig. 4, causes fiber bridging. This fiber bridging gives the T-joint an increased damage tolerance or an ability to carry additional load after initial failure occurs. This fiber bridging is shown schematically in Fig. 7c. The damage progression under increased load causes fiber breakage and pullout as shown in Fig. 7d. Loading beyond this point leads to T-joint catastrophic failure. Figure 8a shows the strain–load plot for strain gage location 2. This gage is located on the edge of the specimen web at the maximum depth of the fiber insertion as

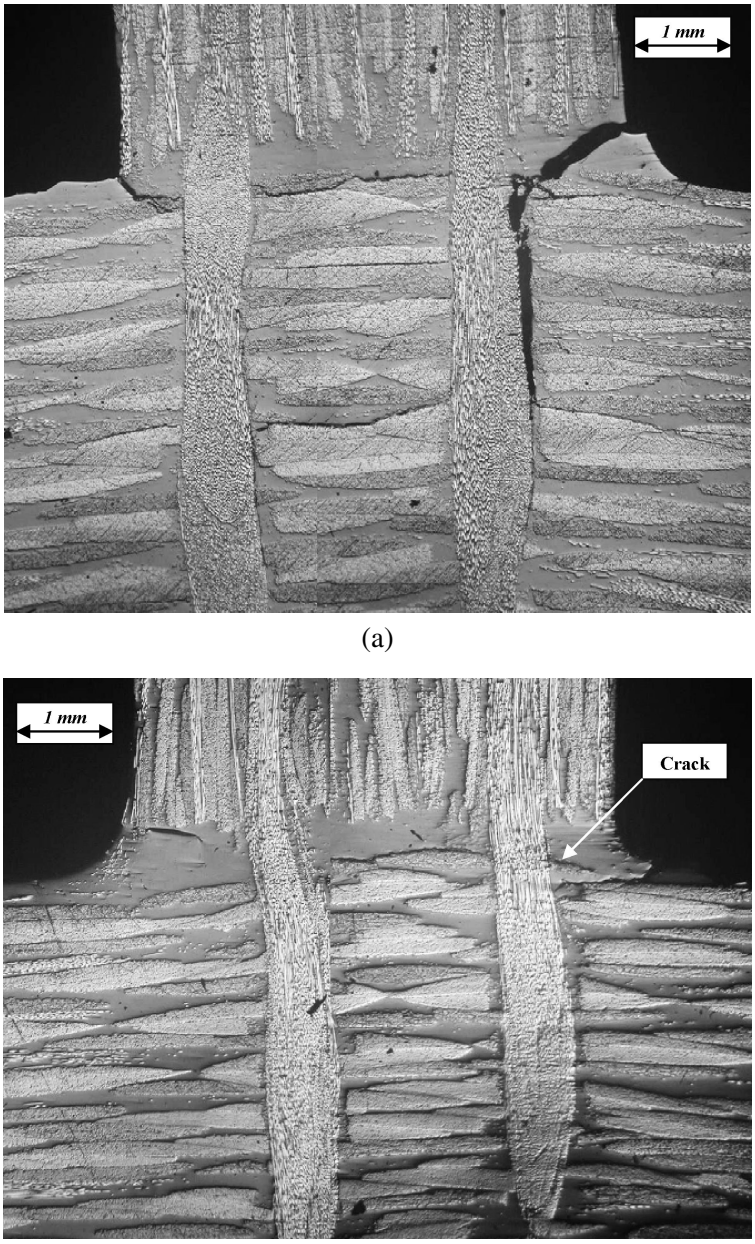

Figure 6. Typical optical micrographs of failed specimens showing interfacial matrix cracking: (a) tension specimen T3 and (b) rail shear specimen S3.

shown in Fig. 8b. Just prior to the initial damage load, a jump in strain is noted. This jump may be attributed to redistribution of load after initial interface matrix failure, causing increased load transfer to the fiber insertions. Also shown is a discrete drop

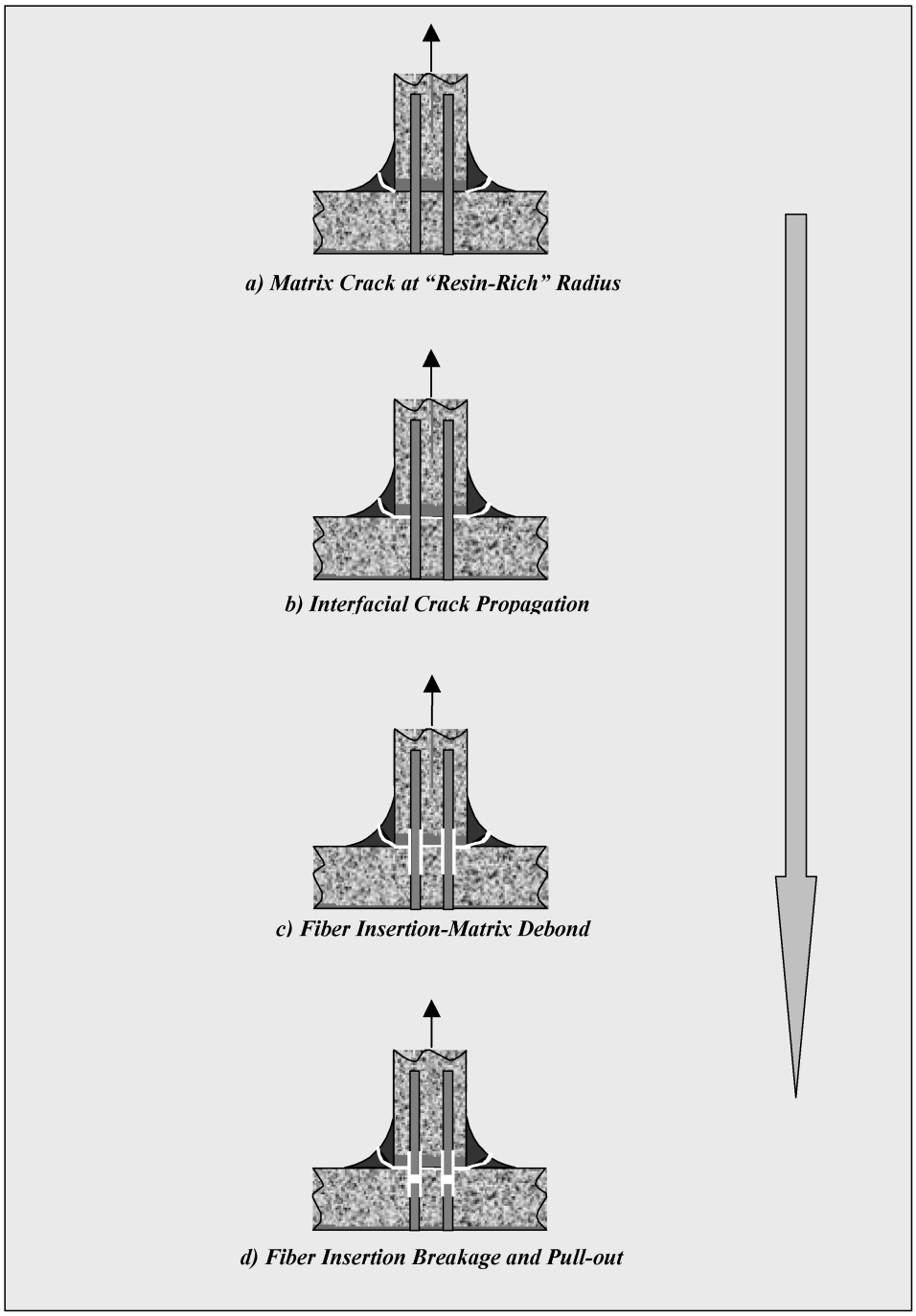

Figure 7. Damage progression under tensile loading.

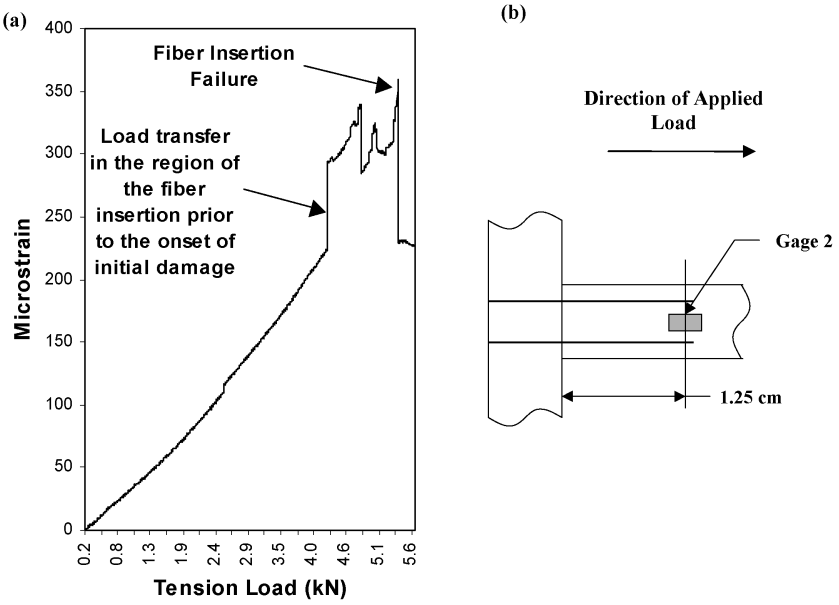

Figure 8. Strain–load record for simple support tension specimen T2 gage location 2: (a) damage progression events and (b) local instrumentation layout.

in strain at T-joint ultimate failure that may be attributed to fiber insertion failure. Several other discrete events are observed at various stages of damage accumulation near ultimate failure.

The mechanical behavior of the T-joint specimens under shear loading is marked by linear elastic behavior, with a sudden onset of damage leading to ultimate failure. This linear behavior is shown in the load–displacement plot of Fig. 5b. Figure 9a–d shows a damage progression schematic for the T-joint subjected to rail shear loading based on experimental, and post-failure analysis of the failed specimens. In this schematic of damage evolution, as shear load is applied to the joint, the matrix deforms elastically, placing the fiber insertions in shear and tension as shown in Fig. 9a. Just prior to T-joint ultimate load, the allowable matrix stress is exceeded and an interfacial matrix crack forms at the web-to-flange interface as shown in Fig. 9b. The matrix crack quickly propagates across the entire surface resulting in additional load transfer to the fiber insertions as shown in Fig. 9c. This matrix crack is observed in the optical micrograph of intact specimens S3 of Fig. 6b. A crack is visible at the web-to-flange interface in the region of the fiber insertions. The onset of damage is very sudden, as indicated by the smooth load–displacement and strain–load records shown in Fig. 4b and Fig. 5b, respectively. As the load is transferred to the fiber insertions, fiber breakage and fiber pullout occurs. Fiber breakage and fiber pullout leads to catastrophic failure of the T-joint as shown in Fig. 9d. This results, in most cases, in complete separation of the web and flange. Figure 10a shows a catastrophically failed rail shear specimen. Failed fiber insertion tows are clearly shown protruding from the web Fig. 10b. Also shown are recesses

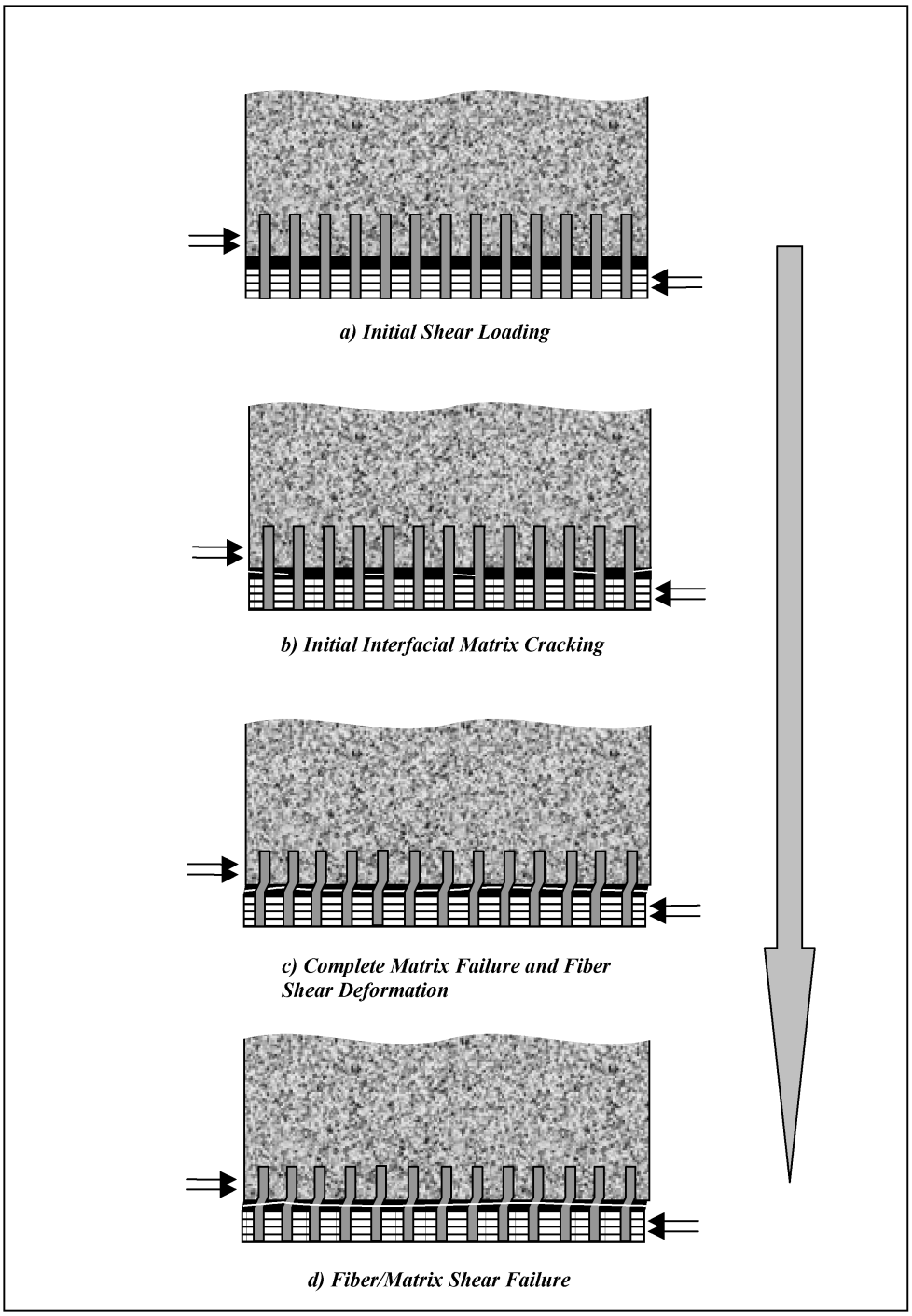

Figure 9. Damage progression under shear loading.

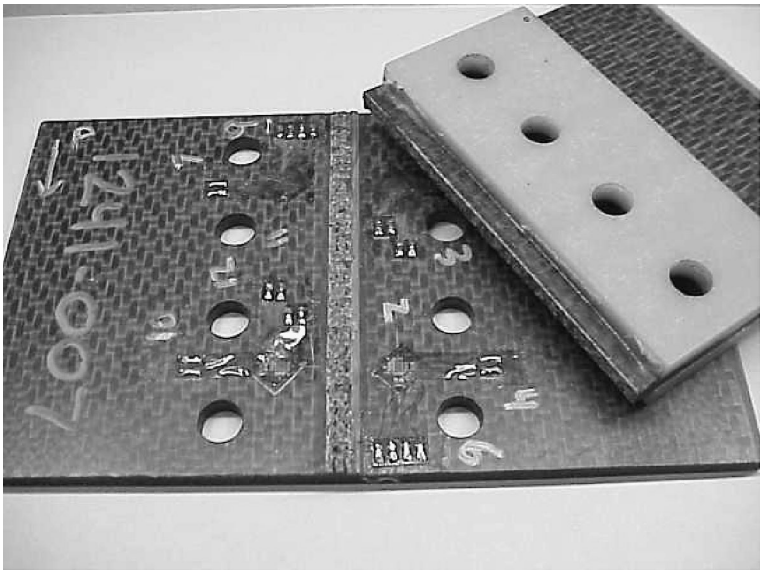

(a)

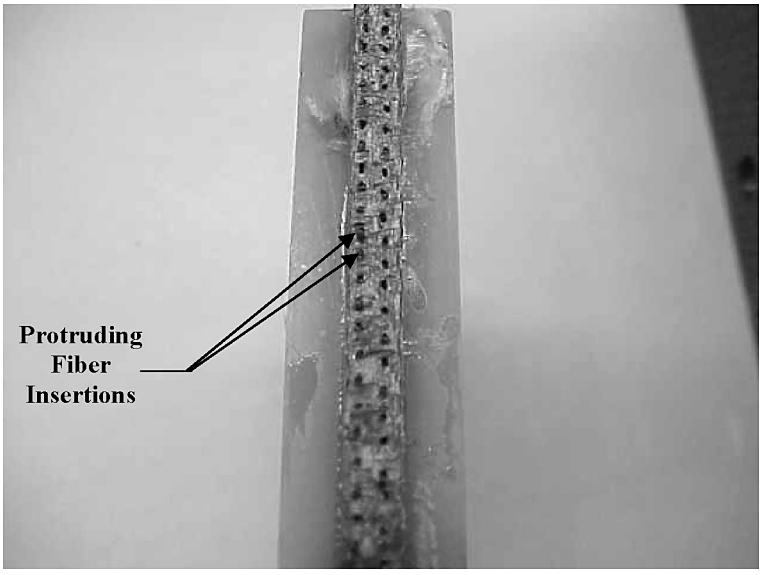

(b)

Figure 10. Photographs of failed rail shear specimen: (a) separated web and flange and (b) web showing protruding fiber insertions.

where fiber insertions pulled out. No continuous loops of fiber insertion are visible, indicating that the web fiber insertion tows broke instead of completely pulling out of the web.

Table 3.
Average damage load and damage ratio summary

Load case	Average initial damage load (kN)	Average ultimate damage load (kN)	Damage load ratio
Flexure [11]	0.57	1.96	3.46
Tension	5.10	5.74	1.13
Rail shear	32.3	34.8	1.08

Table 3 summarizes the average initial damage load, average ultimate damage load, and damage load ratio for the T-joints under flexure, tension, and shear loading. The damage load ratio is defined as the ultimate damage load divided by the initial damage load. Flexure results were reported in a previous investigation by Stickler *et al*. [11]. Several observations may be drawn from these results. Under flexure loading, the damage ratio is high indicating a significant amount of load-carrying capability after initial interfacial matrix failure. Under simple support tension and shear loading, T-joint matrix failure leads to fiber insertion failure. While the fiber insertions are effective beyond the initial failure load under flexure, the fiber insertions are shown to be ineffective beyond the initial failure load under tension and shear.

5. CONCLUSIONS

An experimental study of a new type of T-joint with transverse stitching using a fiber insertion process was undertaken under tension and shear loading. The following are the significant conclusion of this investigation:

- Two distinct regions mark the mechanical behavior under tensile loading. In region one, the load–displacement behavior is nearly linear up to initial failure. Specimens are shown to fail initially by interfacial matrix cracking. In region two, the load–displacement is again linear up to catastrophic failure.
- Onset of T-joint catastrophic failure under tensile loading occurs through fiber insertion breakage and pullout.
- Mechanical loading under rail shear loading is marked by nearly linear behavior up to ultimate failure. Specimens initially fail by interfacial matrix cracking at the web-to-flange interface.
- Onset of T-joint catastrophic failure under shear loading occurs through fiber insertion breakage and pullout with complete separation of the web and flange.
- Based on the damage ratio, while the fiber insertions are effective beyond initial failure under flexure, the fiber insertions are not as effective beyond initial failure under tension and shear.

Acknowledgements

The authors would like to acknowledge The Boeing Company for research support and Albany International Techniweave, Inc., for providing the T-joint specimens and for developing the fiber insertion process.

REFERENCES

1. L. Tong and G. P. Stevens, *Analysis and Design of Structural Bonded Joints*. Kluwer Academic Publishers, Dordrecht, The Netherlands (1999).
2. E. W. Godwin and F. L. Matthews, A review of the strength of joints in fibre-reinforced plastics: Part 1. Mechanically fastened joints, *Composites* **11**, 155–160 (1980).
3. E. W. Godwin and F. L. Matthews, A review of the strength of joints in fibre-reinforced plastics: Part 2. Adhesively bonded joints, *Composites* **13**, 29–37 (1982).
4. L. Tong, L. K. Jain, K. H. Leong, D. Kelly and I. Hertzberg, Failure of transversely stitched RTM lap joints, *Compos. Sci. Technol.* **58**, 221–227 (1998).
5. R. A. Shenoi and F. L. M. Violette, A study of structural composite tee joints in small boats, *J. Compos. Mater.* **24**, 644–665 (1990).
6. E. E. Theotokoglou, Strength of composite T-joints under pull-out loads, *J. Reinforced Plast. Compos.* **16**, 503–518 (1997).
7. H. J. Phillips and R. A. Shenoi, Damage tolerance of laminated tee joints in FRP structures, *Composites Part A* **29**, 465–478 (1998).
8. W. B. Young and M. T. Chuang, Fabrication of T-shaped composite through resin transfer molding, *J. Compos. Mater.* **29**, 2192–2214 (1996).
9. G. Freitas, T. Fusco, T. Campbell, J. Harris and S. Rosenberg, Z-fiber technology and products for enhancing composite design, in: *AGARD Conf. Proc. 590, Bolted/Bonded Joints in Polymeric Composites* (1997).
10. P. B. Stickler, M. Ramulu and P. S. Johnson, Experimental and numerical analysis of transverse stitched T-joints in bending, *Compos. Struct.* **50**, 17–27 (2000).
11. P. B. Stickler, M. Ramulu and B. Van West, Transverse stitched T-joints in bending with PR520 resin, *J. Reinforced Plast. Compos.* **20**, 65–75 (2001).
12. Micromeasurements Group, Inc. Interactive guide to Strain Gage Technology, http://www.measurementsgroup.com (2001).
13. P. B. Stickler, M. Ramulu, S. L. Coguill and M. E. Tuttle, Experimental investigation of T-300/PR520 laminate properties and failure analysis, *J. Adv. Mater.* **36**, 3–11 (2003).